




Article

A Refined Loss Evaluation of a Three-Switch Double Input DC-DC Converter for Hybrid Vehicle Applications

Mario Marchesoni ^{*} , Massimiliano Passalacqua  and Luis Vaccaro 

Department of Electrical, Electronic, Tlc Engineering and Naval Architecture (DITEN), University of Genoa, via all'Opera Pia 11a, 16145 Genova, Italy; massimiliano.passalacqua@edu.unige.it (M.P.); luis.vaccaro@unige.it (L.V.)

* Correspondence: marchesoni@unige.it

Received: 20 November 2019; Accepted: 30 December 2019; Published: 1 January 2020



Abstract: In this paper, an accurate efficiency evaluation of an innovative three-switch double input DC–DC converter for hybrid vehicle applications was carried out. The converter was used to interface two storages, (e.g., supercapacitor and battery) to the DC link. A refined model was created in MATLAB/Simulink Plecs environment and it was used to compare the traditional four-switch converter (i.e., two DC–DC converters in parallel connection) with the innovative three-switch converter. Loss and efficiency contour maps were obtained for both converters and a comparison between them was performed. A prototype of the three-switch converter was realized and used to validate the simulation thermal model by comparing both efficiency and current waveforms obtained with simulations and experimental tests.

Keywords: DC–DC converter; multi-input converter; supercapacitor; battery; hybrid electric vehicle (HEV), efficiency

1. Introduction

The increasing spread of hybrid electric vehicles (HEV) has led to the study and development of new storage systems and storage architectures. As far as battery storages are concerned, lithium batteries have increased their performance, reaching a key role in hybrid medium size car applications [1–6]. On the other hand, many studies have been carried out considering supercapacitor storages on hybrid vehicle, both combining batteries and supercapacitors [7–16] or using only supercapacitors as the storage system [17–28]. Regarding the combined use of batteries and supercapacitors, this configuration matches the pros of both type of storages (i.e., battery high specific energy and supercapacitor high specific power). In order to interface battery and supercapacitor storages with the vehicle DC link (i.e., with motor drive input), a double bidirectional converter is necessary and four full-controlled switches are generally used (Figure 1a) [29–31]. An innovative converter architecture using only three switches is proposed in [32–35] (Figure 1b). Such a converter not only can interface two storage systems with the DC link using a reduced number of switches, but it allows also a higher conversion efficiency. Indeed, on the one hand, reducing the number of switches in multi-input or multi-output converters is a topic of great interest in the technical literature [36–39], on the other, DC–DC converter efficiency is a key point in hybrid vehicles. In [32], a conduction loss comparison between the traditional four-switch converter (4SC) and the innovative three-switch converter (3SC) is carried out; however, regarding switching losses, only a qualitative study was performed. Since the switching losses are generally higher than conduction losses for such types of converters (as is confirmed from the results in Section 4), their accurate evaluation is of primary importance. A study regarding the 3SC efficiency is still missing in the technical literature and is the aim of this paper.

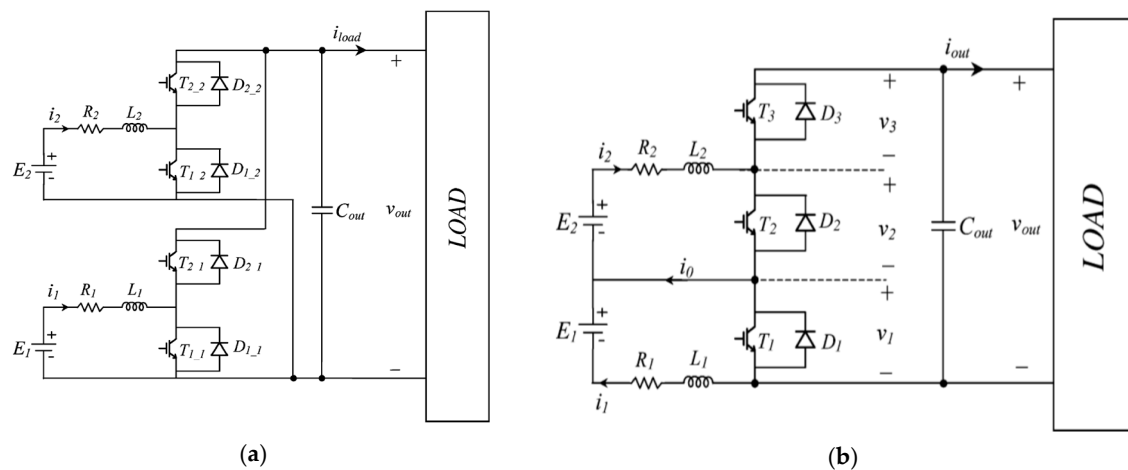


Figure 1. (a) 4SC architecture (b) 3SC architecture.

A refined model in MATLAB/Simulink PLECS environment was developed and used to perform simulations. Moreover, in order to verify the effectiveness of the model, a prototype of the 3SC was built and used to carry out experimental tests.

This paper is structured as follows. In Section 2, 3SC architecture and modulation are presented, together with the MATLAB/Simulink PLECS model. The simulation results regarding converter efficiency are shown in Section 3, and the experimental results are shown in Section 4. Finally, conclusions are carried out in Section 5.

2. Three-Switch Converter (3SC) Architecture and Modulation

The 3SC architecture is shown in Figure 1b. The DC-link voltage (i.e., V_{out} in Figure 1) has to be higher than the sum of E_1 and E_2 , which are the storage voltages (i.e., battery voltage and supercapacitor voltage). The converter is bidirectional and can operate both in boost mode (i.e., power flow from storages to DC-link) or in buck mode (i.e., power flow from DC-link to storages). Battery and supercapacitor power flows in both directions are allowed and are independent of each other. For instance, the converter can work in boost mode for battery storage and in buck mode for supercapacitor storage simultaneously or vice versa.

2.1. Modulation Strategy

If one observes the converter structure, it is easy to notice that the condition in which all switches are closed (on) has to be avoided since it causes DC-link short circuit. Moreover, only one switch can be open at the same time [32]. Indeed, if two or three switches are open, voltages depend on current direction, since currents flow in the free-wheeling diodes. For this reason, if one defines $m_{i_off} = 1 - m_{i_on}$ (where m_{i_on} is the switch on-duty ratio of switch (i)), the relation in Equation (1) has to be satisfied. The relationships between v_1 , v_2 , v_3 and switch on-duty ratios are shown in Figure 2 [32].

$$m_{1_off} + m_{2_off} + m_{3_off} = 1 \quad (1)$$

With reference to Figure 1b, the following relationships (2) can be derived:

$$\begin{aligned} v_1 &= E_1 - R_1 \cdot i_1 - L_1 \cdot \frac{di_1}{dt} \\ v_2 &= E_2 - R_2 \cdot i_2 - L_2 \cdot \frac{di_2}{dt} \\ v_{out} &= v_1 + v_2 + v_3 \end{aligned} \quad (2)$$

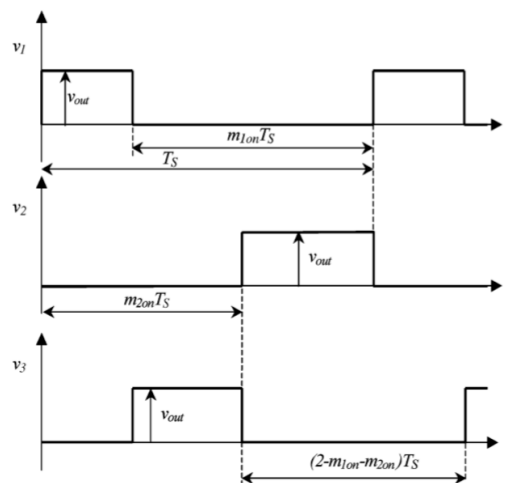


Figure 2. Relationships among v_1 , v_2 and v_3 voltages and switch on-duty ratios.

The v_{out} voltage variation can be neglected during the switching period, so that $v_{out} \approx V_{out}$ and the average voltages V_1 , V_2 and V_3 can be easily obtained:

$$\begin{aligned} V_1 &= (1 - m_{1_on}) \cdot V_{out} \\ V_2 &= (1 - m_{2_on}) \cdot V_{out} \\ V_3 &= (m_{1_on} + m_{2_on} - 1) \cdot V_{out} \end{aligned} \tag{3}$$

The averaged currents I_1 and I_2 can be expressed as in Equation (4) [32]:

$$\begin{aligned} I_1 &= \frac{E_1 - (1 - m_{1_on}) \cdot V_{out}}{R_1} \\ I_2 &= \frac{E_2 - (1 - m_{2_on}) \cdot V_{out}}{R_2} \end{aligned} \tag{4}$$

According to what was previously reported, firing pulse generation logic can be defined as shown in Figure 3a and the resulting firing pulse generation signals are reported in Figure 3b [32].

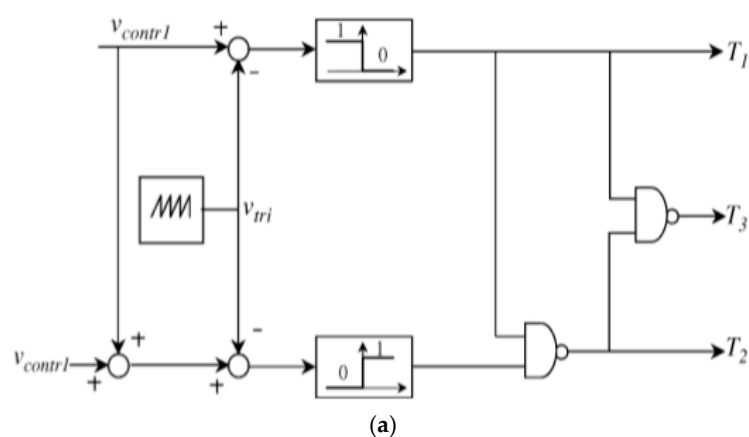


Figure 3. Cont.

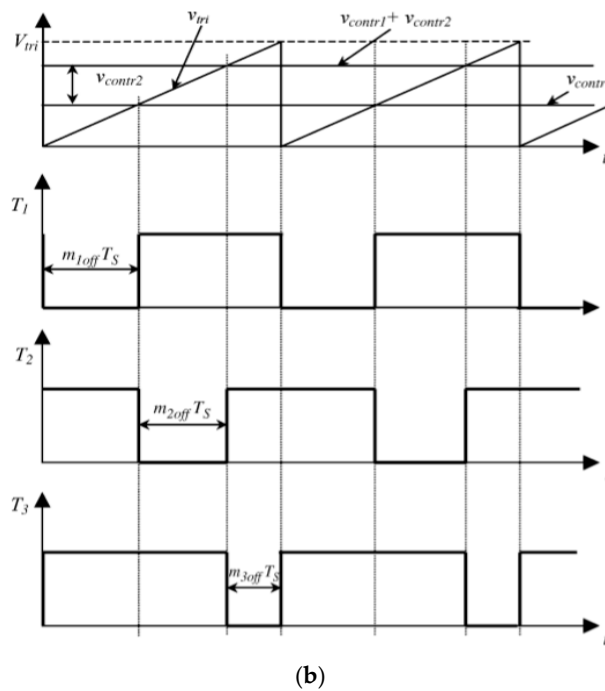


Figure 3. (a) Firing pulse generation logic. (b) Firing pulse generation signals.

2.2. MATLAB/Simulink Plecs Model

In order to establish converter losses, a converter model was created in MATLAB/Simulink Plecs environment, with a thermal model for IGBTs and diodes. Conduction losses were evaluated according to the data shown in Figures 4a and 5a, and the switching losses were evaluated according to the data shown in Figures 4b and 5b. Data were taken from the datasheet provided by the manufacturer of IGBT SKM400GA124D [40]. Indeed, this IGBT was used in the converter prototype. Converter parameters are reported in Table 1, where f_{sw} is the switching frequency; the same parameters were used for both 4SC and 3SC efficiency evaluation. The IGBTs had 1200 V rated voltage and 400 A rated current.

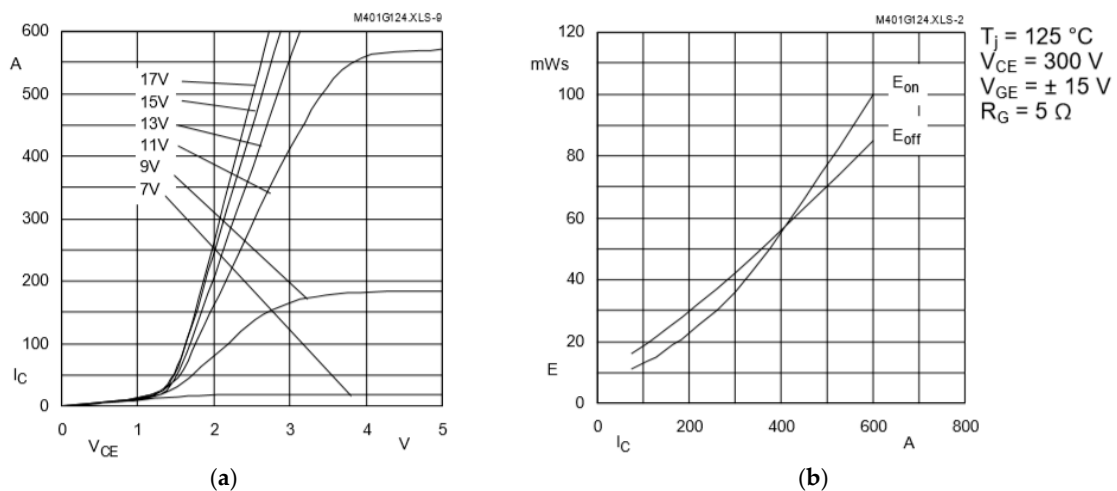


Figure 4. IGBT features. (a) IGBT characteristic (b) IGBT switching losses.

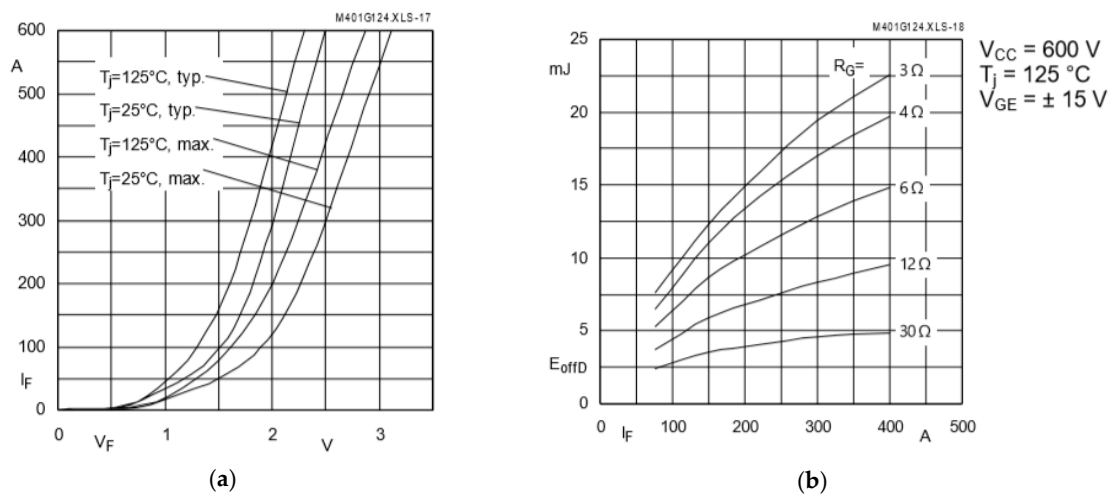


Figure 5. Diode features. (a) Diode characteristic (b) Diode turn-off losses.

Table 1. 3SC parameters.

Parameter	Value
E_1	100 V
L_1	200 μ H
R_1	20 m Ω
E_2	50 V
L_2	100 μ H
R_2	10 m Ω
C_{out}	10 mF
V_{out}	400 V
f_{sw}	10 kHz

Plecs model for the 3SC is reported in Figure 6. Since the simulation time was very low if compared to charging/discharging time, storages were modelled as ideal DC sources. A current source was connected to converter output in order to simulate the load, which can be both active or passive (i.e., injecting or absorbing current). IGBT and diode features of Figures 4 and 5 were implemented in the thermal model of the switches and a heat sink was connected to each of them. Losses were evaluated as the sum of all IGBT losses. Same IGBT thermal model was used in the 4SC model.

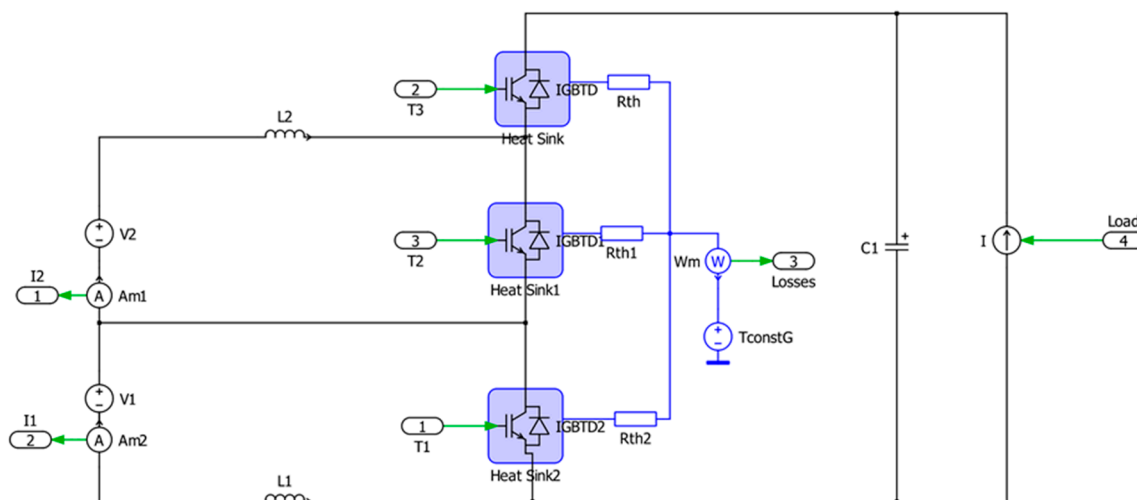


Figure 6. 3SC Plecs model.

3. Simulation Results

A comparison of conduction losses between 4SC and 3SC is shown in [32]; nevertheless, an efficiency analysis considering also switching losses is missing in the literature and therefore, is evaluated in this section. Converter losses (i.e., IGBT and diode conduction losses, IGBT switching losses, diode reverse recovery losses and inductor core losses) were evaluated in all the converters' working ranges. 4SC losses and efficiency contour maps are shown in Figure 7, whereas 3SC contour maps are shown in Figure 8. In Figure 9, losses and efficiency comparisons, i.e., differences, between 4SC and 3SC are reported. When P_1 and P_2 have opposite sign, 4SC losses are slightly lower than 3SC, however, when P_1 and P_2 have the same sign, 3SC losses are significantly lower than 4SC losses. Indeed, observing converter topology in Figure 1b, one can note that current in T1 is i_1 when T3 is off and i_1-i_2 when T2 is off, current in T2 is i_2 when T3 is off and i_2-i_1 when T1 is off, whereas current in T3 is i_1 when T1 is off and i_2 when T2 is off. For this reason, when the currents are concordant, in switches T1 and T2 flows a current which is significantly lower than the one that flows in the switches of a 4SC. Moreover, the condition in which P_1 and P_2 are concordant is the most common condition in hybrid vehicles [32]. Please note that in all the contour maps, P_1 is reported on the X-axis, P_2 is reported on the Y-axis, and losses (or efficiency) are reported on the Z-axis.

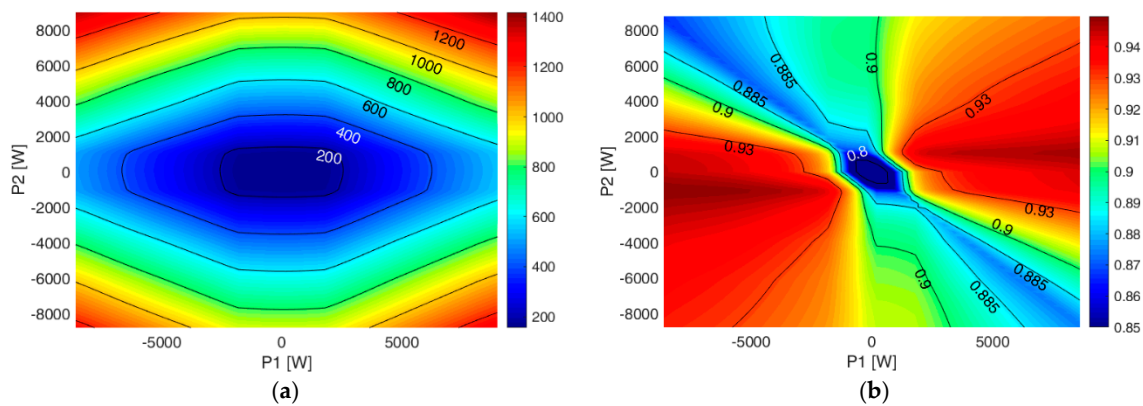


Figure 7. 4SC (a) Losses [W] (b) Efficiency.

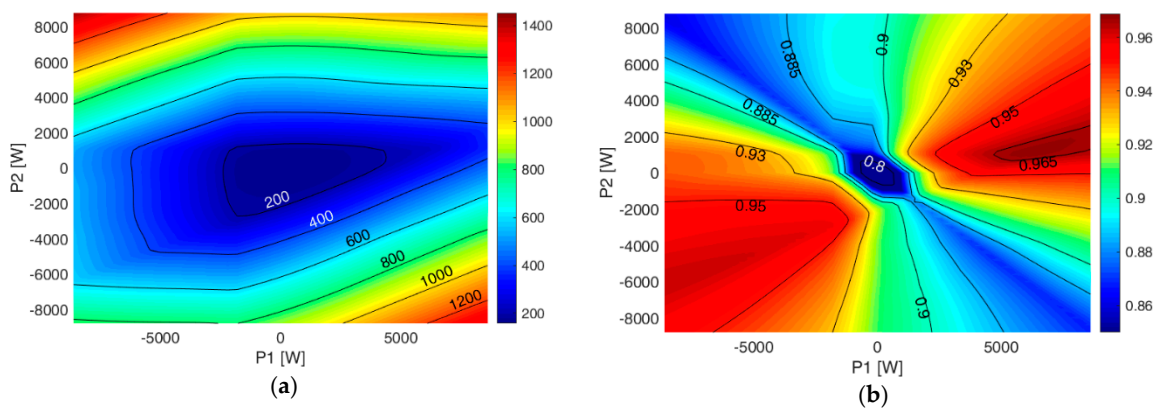


Figure 8. 3SC (a) Losses [W] (b) Efficiency.

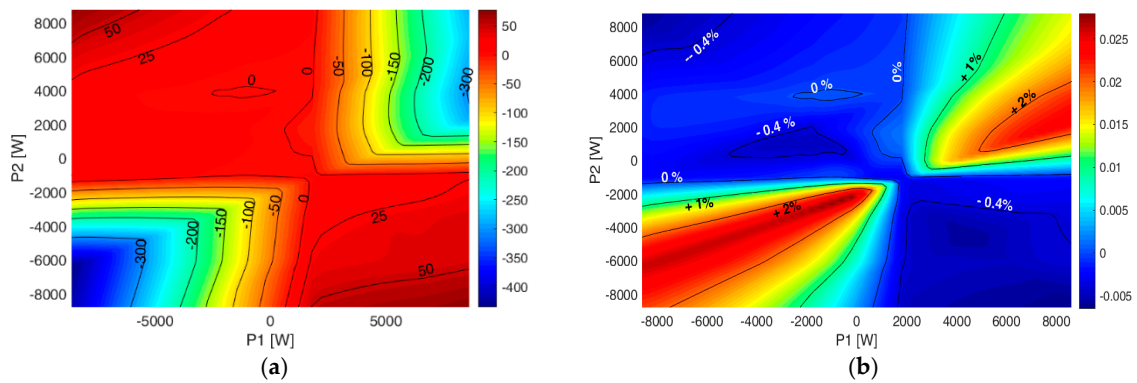


Figure 9. Comparison between 4SC and 3SC (a) 3SC losses—4SC losses [W] (b) 3SC efficiency—4SC efficiency.

4. Experimental Results

4.1. Experimental Test Bench and Validation Approach

In order to validate the simulation model, a prototype of the converter was realized, which is shown in Figures 10 and 11.

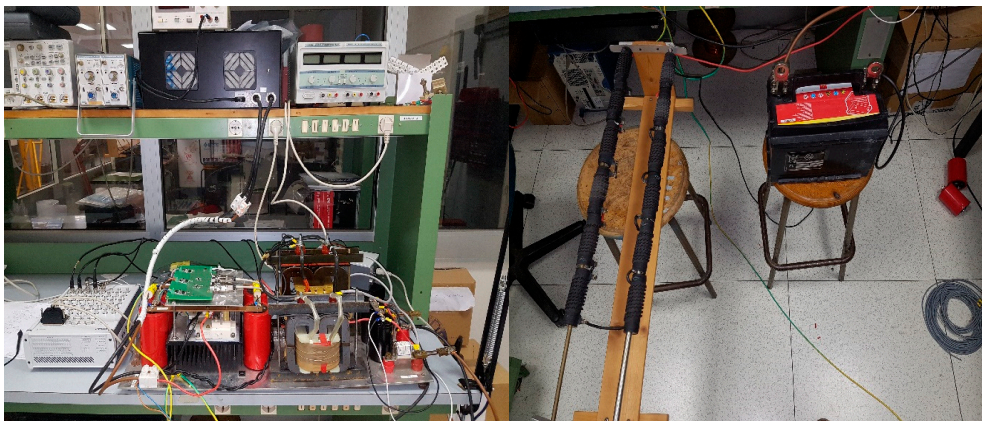


Figure 10. Experimental setup.

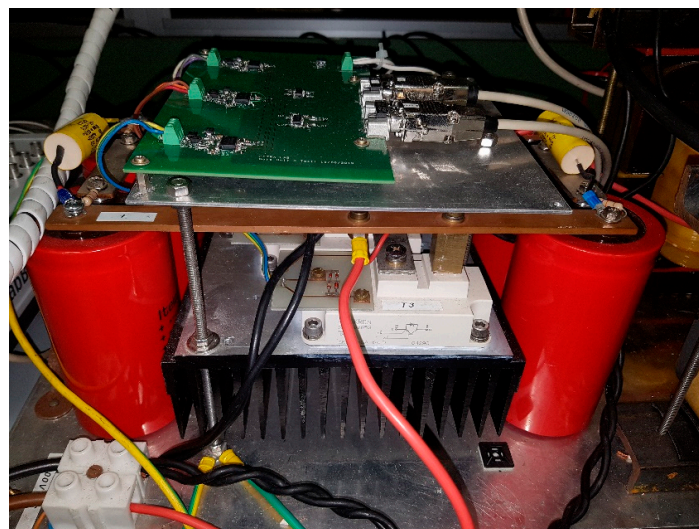


Figure 11. Converter prototype.

The prototype has three IGBTs SKM400GA124D, as in the simulation model, but it has different inductance and voltage values, as reported in Table 2. The aim of the prototype was to validate the simulation model, therefore, other simulations were performed with voltage and inductance values used in the converter prototype. Indeed, the converter efficiency was evaluated at first in the rated working points, in order to evaluate converter potential performance; however, since the experimental tests were performed at lower voltages and currents, simulations were performed also at the same values as in the experimental tests. In this way, it was possible to compare current waveforms and efficiency obtained via simulations with the ones obtained via experimental tests. A supercapacitor was used as E_2 (with a voltage of about 22 V) whereas a battery was used as E_1 (with a voltage of about 12 V). A 166 Ω resistor was connected to the DC-link and could be disconnected to test the converter only with power exchange between storages. Due to this configuration, the prototype could not be tested in full-buck operation (i.e., both, storages in charging condition) but the other working operations could all be tested: full-boost operation (i.e., both storages in discharging mode) and buck-boost operation (i.e., one storage in charging mode with the other one in discharging mode and vice versa).

Table 2. Prototype parameters.

Parameter	Value
IGBTs	SKM400GA124D
E_1	12 V
L_1	330 μ H
E_2	22 V
L_2	950 μ H
C_{out}	10 mF
V_{out}	100 V
f_{sw}	10 kHz

The aim of the experimental tests was to validate the simulation model with two different approaches:

1. Comparing the current waveforms obtained via simulations with the ones obtained via experimental tests.
2. Comparing the efficiency obtained via simulations with the one obtained via experimental tests.

Both approaches were useful for model validation. Indeed, since $V_{ce} = V_{ce}(I_c)$, $V_f = V_f(I_f)$, $E_{on} = E_{on}(I_c)$, $E_{off} = E_{off}(I_c)$ and $E_{offd} = E_{offd}(I_f)$ are all monotonous increasing functions (Figures 4 and 5), a reduction in switching and/or conduction losses is inevitably caused by a reduction in current values during switching or conduction. For this reason, it is important to verify that the current waveforms obtained with simulations are in accordance with the current waveforms obtained with the experimental tests. On the other hand, it is important to verify that the efficiency obtained with the prototype converter is comparable with the one obtained with simulation, so that the efficiency increase (or decrease) moving from 4SC to 3SC can be considered sufficiently accurate. However, evaluating only this second aspect would be not sufficient; indeed, many conditions intervene in real applications, therefore, it is obvious that the efficiency evaluation with simulation cannot be very precise. Nevertheless, if the current waveforms are well simulated, the efficiency variation between 4SC and 3SC is accurate, thanks to the monotony of the previous functions. Definitively, even if the absolute converter efficiency cannot be modelled precisely with simulations, the efficiency variation, between 4SC and 3SC, can be modelled precisely if the current waveforms are correctly simulated.

4.2. Experimental Results

Three different tests were performed, which correspond to the three different working conditions. Test 1 (Table 3) was with the converter in full-boost operation (i.e., both storages in discharging mode),

whereas Tests 2 and 3 were in buck-boost operations: in Test 2, the battery was discharging and the supercapacitor was charging; in Test 3, the battery was charging and the supercapacitor was discharging. In all three configurations, there was a load of 0.6 A on the DC-link. In Table 4, simulation losses are shown, together with the efficiency evaluated via simulations and the efficiency evaluated with the experimental tests. The efficiency was evaluated according to the equations in Table 3.

Table 3. Efficiency evaluation.

Test	Efficiency via Simulation	Efficiency via Experimental Test
1	$\eta = \frac{V_{out} \cdot I_{out}}{V_{out} \cdot I_{out} + Losses}$	$\eta = \frac{V_{out} \cdot I_{out}}{V_1 \cdot I_1 + V_2 \cdot I_2}$
2	$\eta = \frac{V_{out} \cdot I_{out} + V_2 \cdot I_2 }{V_{out} \cdot I_{out} + V_2 \cdot I_2 + Losses}$	$\eta = \frac{V_{out} \cdot I_{out} + V_2 \cdot I_2 }{V_1 \cdot I_1}$
3	$\eta = \frac{V_{out} \cdot I_{out} + V_1 \cdot I_1 }{V_{out} \cdot I_{out} + V_1 \cdot I_1 + Losses}$	$\eta = \frac{V_{out} \cdot I_{out} + V_1 \cdot I_1 }{V_2 \cdot I_2}$

From Table 4, it can be noticed that the thermal model in MATLAB/Simulink Plecs well represents the converter efficiency; indeed, the efficiency obtained with simulations is very close to the one obtained with experimental results, in all the tests.

Table 4. Experimental test current values and efficiency.

Test	I 1 (V1)	I 2 (V2)	I out (Vout)	Simulation Losses (of which for Conduction)	η Simulation	η Experimental
1	6 A (12 V)	0.5 A (22 V)	0.6 A (100 V)	21.5 W (1.2 W)	74%	72%
2	14 A (12 V)	−2 A (22 V)	0.6 A (100 V)	70 W (9 W)	60%	62%
3	−2 A (12 V)	5 A (22 V)	0.6 A (100 V)	27.6 W (1.5 W)	75%	76%

The 3SC efficiency is greater than 90% in the majority of the working points, as can be seen in Figure 8b, even if one has to note that converter efficiency shown in Table 4 is quite low. The cause of such a low efficiency is that, in the experimental tests, the converter did not work in conditions close to the rated working points. The evaluation of converter efficiency in the rated working points is carried out in Section 3 via simulation. The aim of the experimental test was to validate the Plecs model and, especially, the thermal model used in it. Moreover, an error of 2% between simulated and experimentally measured efficiency seems to be quite high. However, one has to consider the loss percent error. Indeed, an error of 2% on efficiency while efficiency is 96% corresponds to an error of 50% on the losses, which is not tolerable. In the results in Table 4, instead, the worst case is an error of 2% with 74% efficiency, which is equivalent to an error of about 7% on the losses, which is significantly low considering all the non-idealities of a real converter.

In Figures 12–14, simulation and experimental current waveforms in the three different tests are plotted. One can note that the simulation model well represents the converter behaviour. Indeed, very similar results were obtained from simulations and experimental tests.

Ultimately, the converter is well modelled since, on the one hand, the converter efficiency obtained via simulations is close to the measured one and also because the current waveforms are very similar in the simulations and experimental tests. All in all, the two approaches of validation described in Section 4.1 are both verified and the results obtained in Section 3 are therefore validated.

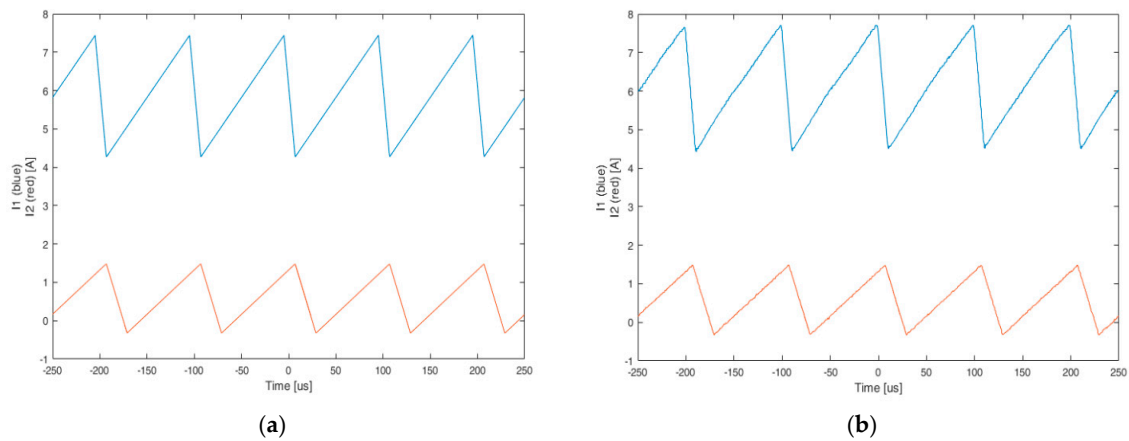


Figure 12. Current waveforms in Test 1 (a) simulation (b) experimental.

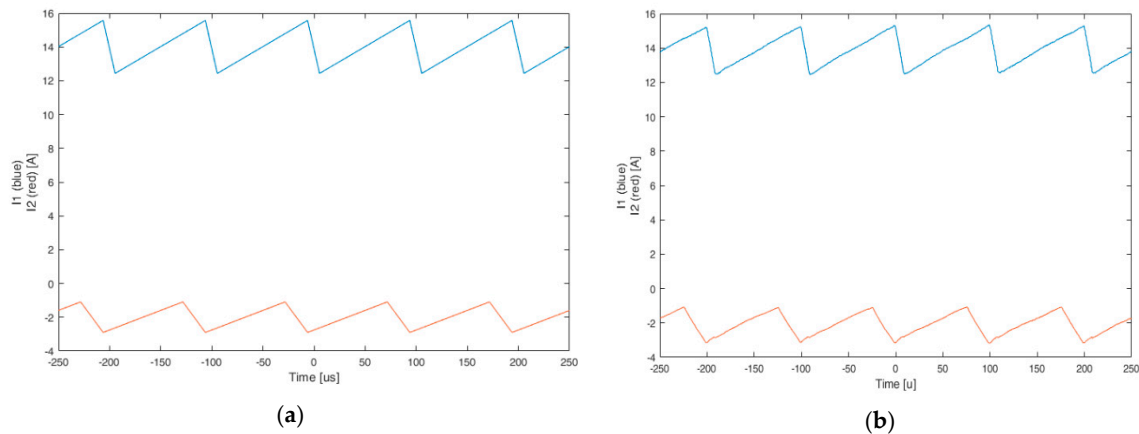


Figure 13. Current waveforms in Test 2 (a) simulation (b) experimental.

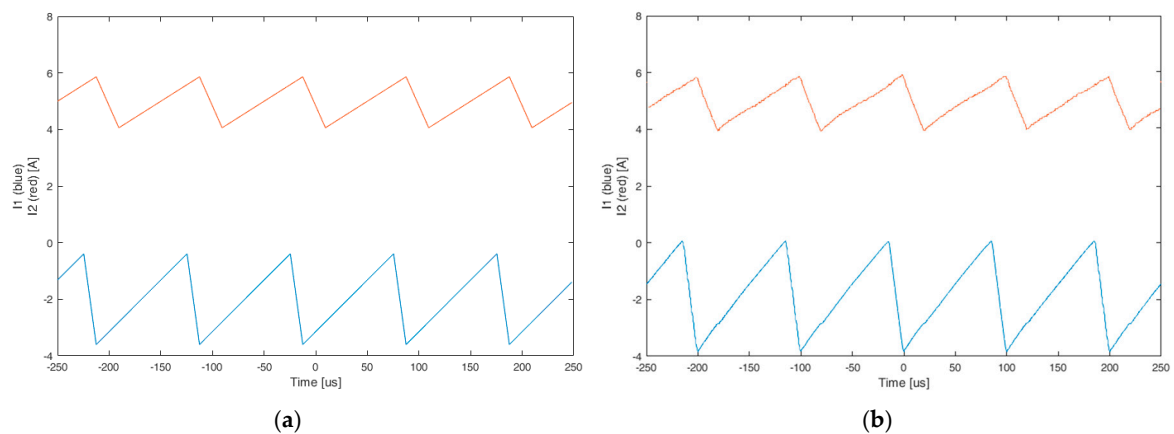


Figure 14. Current waveforms in Test 3 (a) simulation (b) experimental.

5. Conclusions

In this paper, the efficiency of an innovative three-switch DC-DC converter for hybrid vehicle applications was analysed. A refined model of the converter was created in MATLAB/Simulink PLECS environment. The model was used to evaluate the efficiency of both the traditional four-switch converter (i.e., two DC-DC converters in parallel connection) and the three-switch converter, in order to compare them. This study shows that not only does the three-switch converter use a reduced number

of IGBTs, but the efficiency is significantly higher when the power flows of battery and supercapacitor are concordant (which is the most common condition).

The Plecs model was validated by comparing the results obtained via simulations with the results obtained with the experimental tests. The tests were performed on a prototype converter that has the same switches used to perform the simulations.

The experimental tests show an efficiency very close to the simulated one and moreover, the current waveforms obtained with the experimental tests are very similar to the ones obtained with simulations. The simulation model is therefore validated and the efficiency comparison between the four-switch converter and the three-switch converter can be considered very accurate.

Author Contributions: Conceptualization, M.M. and L.V.; Data curation, M.P.; Formal analysis, M.P.; Funding acquisition, M.M.; Investigation, M.P.; Methodology, L.V.; Resources, L.V.; Software, M.P.; Supervision, M.M.; Validation, L.V.; Writing—original draft, M.P.; Writing—review & editing, M.M. All authors have read and agreed to the published version of the manuscript.

Funding: This research received no external funding.

Conflicts of Interest: The authors declare no conflict of interest.

References

- Burress, T.A.; Campbell, S.L.; Coomer, C.L.; Ayers, C.W.; Wereszczak, A.A.; Cunningham, J.P.; Marlino, L.D.; Seiber, L.E.; Lin, H.T. *Evaluation of the 2010 toyota prius hybrid synergy drive system. Power Electronics and Electric Machinery Research Facility*; Technical Report ORNL/TM2010/253; Oak Ridge National Laboratory (ORNL): Oak Ridge, TN, USA, 2011.
- Zhang, X.; Peng, H.; Wang, H.; Ouyang, M. Hybrid lithium iron phosphate battery and lithium titanate battery systems for electric buses. *IEEE Trans. Veh. Technol.* **2018**, *67*, 956–965. [[CrossRef](#)]
- Lanzarotto, D.; Marchesoni, M.; Passalacqua, M.; Prato, A.P.; Repetto, M. Overview of different hybrid vehicle architectures. *IFAC-PapersOnLine* **2018**, *51*, 218–222. [[CrossRef](#)]
- Sinkaram, C.; Asirvadam, V.S.; Nor, N.B.M. Capacity study of lithium ion battery for hybrid electrical vehicle (HEV) a simulation approach. In Proceedings of the 2013 IEEE International Conference on Signal and Image Processing Applications, Melaka, Malaysia, 8–10 October 2013; pp. 112–116.
- Xiong, R.; He, H.; Sun, F.; Zhao, K. Online estimation of peak power capability of li-ion batteries in electric vehicles by a hardware-in-loop approach. *Energies* **2012**, *5*, 1455–1469. [[CrossRef](#)]
- Bonfiglio, A.; Lanzarotto, D.; Marchesoni, M.; Passalacqua, M.; Procopio, R.; Repetto, M. Electrical-loss analysis of power-split hybrid electric vehicles. *Energies* **2017**, *10*, 2142. [[CrossRef](#)]
- Camara, M.B.; Gualous, H.; Gustin, F.; Berthon, A.; Dakyo, B. Dc/dc converter design for supercapacitor and battery power management in hybrid vehicle applications—polynomial control strategy. *IEEE Trans. Ind. Electron.* **2010**, *57*, 587–597. [[CrossRef](#)]
- Golchoubian, P.; Azad, N.L. Real-time nonlinear model predictive control of a battery–supercapacitor hybrid energy storage system in electric vehicles. *IEEE Trans. Veh. Technol.* **2017**, *66*, 9678–9688. [[CrossRef](#)]
- Liu, S.; Peng, J.; Li, L.; Gong, X.; Lu, H. A mpc based energy management strategy for battery-supercapacitor combined energy storage system of HEV. In Proceedings of the 2016 35th Chinese Control Conference (CCC), Chengdu, China, 27–29 July 2016; pp. 8727–8731.
- Cao, J.; Emadi, A. A new battery/ultracapacitor hybrid energy storage system for electric, hybrid, and plug-in hybrid electric vehicles. *IEEE Trans. Power Electronics* **2012**, *27*, 122–132.
- Sampietro, J.L.; Puig, V.; Costa-Castelló, R. Optimal sizing of storage elements for a vehicle based on fuel cells, supercapacitors, and batteries. *Energies* **2019**, *12*, 925. [[CrossRef](#)]
- Cheng, L.; Wang, W.; Wei, S.; Lin, H.; Jia, Z. An improved energy management strategy for hybrid energy storage system in light rail vehicles. *Energies* **2018**, *11*, 423. [[CrossRef](#)]
- Zhang, C.; Min, H.; Yu, Y.; Wang, D.; Luke, J.; Opila, D.; Saxena, S. Using cpe function to size capacitor storage for electric vehicles and quantifying battery degradation during different driving cycles. *Energies* **2016**, *9*, 903. [[CrossRef](#)]
- Zhang, Q.; Deng, W. An adaptive energy management system for electric vehicles based on driving cycle identification and wavelet transform. *Energies* **2016**, *9*, 341. [[CrossRef](#)]

15. Odeim, F.; Roes, J.; Heinzl, A. Power management optimization of an experimental fuel cell/battery/supercapacitor hybrid system. *Energies* **2015**, *8*, 6302–6327. [[CrossRef](#)]
16. Marchesoni, M.; Savio, S. Reliability analysis of a fuel cell electric city car. In Proceedings of the 2005 European Conference on Power Electronics and Applications, Dresden, Germany, 11–14 September 2005; p. 10.
17. Passalacqua, M.; Lanzarotto, D.; Repetto, M.; Marchesoni, M. Advantages of using supercapacitors and silicon carbide on hybrid vehicle series architecture. *Energies* **2017**, *10*, 920. [[CrossRef](#)]
18. Zhao, Y.; Yao, J.; Zhong, Z.m.; Sun, Z.c. The research of powertrain for supercapacitor-based series hybrid bus. In Proceedings of the 2008 IEEE Vehicle Power and Propulsion Conference, Harbin, China, 3–5 September 2008; pp. 1–4.
19. Wu, W.; Partridge, J.; Bucknall, R. Development and evaluation of a degree of hybridisation identification strategy for a fuel cell supercapacitor hybrid bus. *Energies* **2019**, *12*, 142. [[CrossRef](#)]
20. Passalacqua, M.; Lanzarotto, D.; Repetto, M.; Vaccaro, L.; Bonfiglio, A.; Marchesoni, M. Fuel economy and ems for a series hybrid vehicle based on supercapacitor storage. *IEEE Trans. Power Electron.* **2019**, *34*, 9966–9977. [[CrossRef](#)]
21. Moreno, J.; Ortúzar, M.E.; Dixon, J.W. Energy-management system for a hybrid electric vehicle, using ultracapacitors and neural networks. *IEEE Trans. Ind. Electron.* **2006**, *53*, 614–623. [[CrossRef](#)]
22. Passalacqua, M.; Carpita, M.; Gavin, S.; Marchesoni, M.; Repetto, M.; Vaccaro, L.; Wasterlain, S. Supercapacitor storage sizing analysis for a series hybrid vehicle. *Energies* **2019**, *12*, 1759. [[CrossRef](#)]
23. Partridge, J.; Abouelamaimen, D.I. The role of supercapacitors in regenerative braking systems. *Energies* **2019**, *12*, 2683. [[CrossRef](#)]
24. Thounthong, P.; Chunkag, V.; Sethakul, P.; Davat, B.; Hinaje, M. Comparative study of fuel-cell vehicle hybridization with battery or supercapacitor storage device. *IEEE Trans. Veh. Technol.* **2009**, *58*, 3892–3904. [[CrossRef](#)]
25. Fadil, H.E.; Giri, F.; Guerrero, J.M.; Tahri, A. Modeling and nonlinear control of a fuel cell/supercapacitor hybrid energy storage system for electric vehicles. *IEEE Trans. Veh. Technol.* **2014**, *63*, 3011–3018. [[CrossRef](#)]
26. Passalacqua, M.; Lanzarotto, D.; Repetto, M.; Marchesoni, M. Conceptual design upgrade on hybrid powertrains resulting from electric improvements. *Int. J. Transp. Dev. Integr.* **2018**, *2*, 146–154. [[CrossRef](#)]
27. Zhang, R.; Tao, J.; Zhou, H. Fuzzy optimal energy management for fuel cell and supercapacitor systems using neural network based driving pattern recognition. *IEEE Trans. Fuzzy Syst.* **2019**, *27*, 45–57. [[CrossRef](#)]
28. Lanzarotto, D.; Passalacqua, M.; Repetto, M. Energy comparison between different parallel hybrid vehicles architectures. *Int. J. Energy Prod. Manag.* **2017**, *2*, 370–380. [[CrossRef](#)]
29. Lukic, S.M.; Wirasingha, S.G.; Rodriguez, F.; Cao, J.; Emadi, A. Power management of an ultracapacitor/battery hybrid energy storage system in an HEV. In Proceedings of the 2006 IEEE Vehicle Power and Propulsion Conference, Windsor, UK, 6–8 September 2006; pp. 1–6.
30. Onar, O.C.; Khaligh, A. A novel integrated magnetic structure based dc/dc converter for hybrid battery/ultracapacitor energy storage systems. *IEEE Trans. Smart Grid* **2012**, *3*, 296–307. [[CrossRef](#)]
31. Shen, J.; Khaligh, A. A supervisory energy management control strategy in a battery/ultracapacitor hybrid energy storage system. *IEEE Trans. Transp. Electrification* **2015**, *1*, 223–231. [[CrossRef](#)]
32. Marchesoni, M.; Vacca, C. New dc–dc converter for energy storage system interfacing in fuel cell hybrid electric vehicles. *IEEE Trans. Power Electron.* **2007**, *22*, 301–308. [[CrossRef](#)]
33. Carpaneto, M.; Ferrando, G.; Marchesoni, M.; Vacca, C. The average switch model of a new double-input dc/dc boost converter for hybrid fuel-cell vehicles. In Proceedings of the IEEE International Symposium on Industrial Electronics (ISIE 2005), Dubrovnik, Croatia, 20–23 June 2005; pp. 601–607.
34. Carpaneto, M.; Ferrando, G.; Marchesoni, M.; Savio, S. A new conversion system for the interface of generating and storage devices in hybrid fuel-cell vehicles. In Proceedings of the IEEE International Symposium on Industrial Electronics (ISIE 2005), Dubrovnik, Croatia, 20–23 June 2005; pp. 1477–1482.
35. Barabino, G.; Carpaneto, M.; Comacchio, L.; Marchesoni, M.; Novella, G. A new energy storage and conversion system for boat propulsion in protected marine areas. In Proceedings of the 2009 International Conference on Clean Electrical Power, Capri, Italy, 9–11 June 2009; pp. 363–369.
36. Chen, G.; Jin, Z.; Deng, Y.; He, X.; Qing, X. Principle and topology synthesis of integrated single-input dual-output and dual-input single-output dc–dc converters. *IEEE Trans. Ind. Electron.* **2018**, *65*, 3815–3825. [[CrossRef](#)]

37. Wai, R.; Lin, C.; Chen, B. High-efficiency dc–dc converter with two input power sources. *IEEE Trans. Power Electron.* **2012**, *27*, 1862–1875. [[CrossRef](#)]
38. Liu, Y.; Chen, Y. A systematic approach to synthesizing multi-input dc–dc converters. *IEEE Trans. Power Electron.* **2009**, *24*, 116–127. [[CrossRef](#)]
39. Ganjavi, A.; Ghoreishy, H.; Ahmad, A.A. A novel single-input dual-output three-level dc–dc converter. *IEEE Trans. Ind. Electron.* **2018**, *65*, 8101–8111. [[CrossRef](#)]
40. Semikron. Available online: <https://www.semikron.com> (accessed on 31 December 2019).



© 2020 by the authors. Licensee MDPI, Basel, Switzerland. This article is an open access article distributed under the terms and conditions of the Creative Commons Attribution (CC BY) license (<http://creativecommons.org/licenses/by/4.0/>).